THE JOURNAL OF BIOLOGICAL CHEMISTRY
Vol. 276, No. 24, Issue of June 15, pp. 21562–21570, 2001
© 2001 by The American Society for Biochemistry and Molecular Biology, Inc.
Printed in U.S.A.

Early-onset Amyloid Deposition and Cognitive Deficits in Transgenic Mice Expressing a Double Mutant Form of Amyloid Precursor Protein 695*

Received for publication, January 25, 2001, and in revised form, March 9, 2001
Published, JBC Papers in Press, March 15, 2001, DOI 10.1074/jbc. M100710200

M. Azhar Chishti,[a] Dun-Shen Yang,[a] Christopher Janus,[a] Amie L. Phinney,[a,b] Patrick Horne,[a] Jacqueline Pearson,[a] Robert Strome,[a] Noah Zuker,[a] James Loukides,[a] Janet French,[a] Sherry Turner,[c] Gianluca Lozza,[d] Mariagrazia Grilli,[d] Suzanne Kunicki,[e,f] Céline Morissette,[e] Julie Paquette,[e] Francine Gervais,[e], Catherine Bergeron,[a,g,h] Paul E. Fraser,[a,i] George A. Carlson,[c] Peter St. George-Hyslop,[a,j,h] and David Westaway[a,g,k]

From the [a]Centre for Research in Neurodegenerative Diseases, the [g]Department of Laboratory Medicine and Pathobiology, the [i]Department of Medical Biophysics, the [j]Department of Medicine (Division of Neurology), [h]University Health Network, University of Toronto, Toronto, Ontario M5S 3H2, Canada, [c]McLaughlin Research Institute, Great Falls, Montana 59405-4900, [d]Schering-Plough Research Institute, Milan, Italy, and [e]Neurochem Inc., Ville St.-Laurent, Montreal, Quebec H4S 2A1, Canada

We have created early-onset transgenic (Tg) models by exploiting the synergistic effects of familial Alzheimer's disease mutations on amyloid β-peptide (Aβ) biogenesis. TgCRND8 mice encode a double mutant form of amyloid precursor protein 695 (KM670/671NL+V717F) under the control of the PrP gene promoter. Thioflavine S-positive Aβ amyloid deposits are present at 3 months, with dense-cored plaques and neuritic pathology evident from 5 months of age. TgCRND8 mice exhibit 3,200–4,600 pmol of Aβ42 per g brain at age 6 months, with an excess of Aβ42 over Aβ40. High level production of the pathogenic Aβ42 form of Aβ peptide was associated with an early impairment in TgCRND8 mice in acquisition and learning reversal in the reference memory version of the Morris water maze, present by 3 months of age. Notably, learning impairment in young mice was offset by immunization against Aβ42 (Janus, C., Pearson, J., McLaurin, J., Mathews, P. M., Jiang, Y., Schmidt, S. D., Chishti, M. A., Horne, P., Heslin, D., French, J., Mount, H. T. J., Nixon, R. A., Mercken, M., Bergeron, C., Fraser, P. E., St. George-Hyslop, P., and Westaway, D. (2000) *Nature* 408, 979–982). Amyloid deposition in TgCRND8 mice was enhanced by the expression of presenilin 1 transgenes including familial Alzheimer's disease mutations; for mice also expressing a M146L+L286V presenilin 1 transgene, amyloid deposits were apparent by 1 month of age. The Tg mice described here suggest a potential to investigate aspects of Alzheimer's disease pathogenesis, prophylaxis, and therapy within short time frames.

Alzheimer's disease, the most common cause of dementia, has a complex etiology involving both genetic and environmental determinants. It is characterized by cerebral amyloid deposits formed from the amyloid β-peptide (Aβ),[1] neuronal loss, and intracellular deposits denoted neurofibrillary tangles (NFTs), aggregations of hyper-phosphorylated forms of the microtubule-associated protein tau (τ). Genetic analyses of diverse familial Alzheimer's disease (FAD) kindreds indicate biosynthesis of the amyloid β-peptide (Aβ), generated by secretase-mediated endoproteolysis of the amyloid precursor protein (APP), is a common denominator in inherited forms of the disease. In the case of chromosome 21-linked FAD kindreds, mutations in APP are found in close proximity to the endoprotease sites where Aβ is excised by the action of β- and γ-secretases (2–6). Mutations in presenilins 1 and 2 are thought to enhance cleavage of APP at the γ-secretase site (7–9). Finally, the ϵ4 allele of the ApoE gene, which is correlated with increased susceptibility to late-onset AD (10), is found to enhance the formation of mature plaques in certain APP transgenic mice (11). These genetic data indicate elevated Aβ biogenesis or accumulation is likely a crucial pathogenic event in all forms of AD (*i.e.* both familial and sporadic AD). This conclusion finds a parallel in studies indicating that Aβ is neurotoxic (12–14).

Since there are no naturally occurring rodent forms of AD, there has been great interest in creating accurate transgenic facsimiles of this disease. Such disease models have the potential to stratify pathogenic events and practical utility for testing interventions directed against synthesis or deposition of the Aβ peptide. However, despite intense effort, remarkably few models exist (reviewed in Ref. 15). Some models fail to produce APP and/or its metabolites by physiologically appropriate path-

* This work was supported in part by the Canadian Institutes for Health Research, the Ontario Mental Health Foundation, The Howard Hughes Medical Institute, Natural Sciences and Engineering Research Council of Canada, The Scottish Rite Foundation, the Alzheimer Society of Ontario, the National Institute on Aging, and the Fraternal Order of Eagles. The costs of publication of this article were defrayed in part by the payment of page charges. This article must therefore be hereby marked "*advertisement*" in accordance with 18 U.S.C. Section 1734 solely to indicate this fact.

[b] Supported by Canadian Institutes for Health Research post-doctoral fellowship.

[f] Supported by Natural Sciences and Engineering Research Council of Canada post-doctoral fellowships.

[k] To whom correspondence should be addressed: University of Toronto, Center for Research in Neurodegenerative Diseases, Tanz Neuroscience Bldg., 6 Queen's Park Crescent West, Toronto, Ontario M5S 3H2, Canada. Tel.: 416-978-1556; Fax: 416-978-1878; E-mail: david.westaway@utoronto.ca.

[1] The abbreviations used are: Aβ, amyloid β-peptide; FAD, familial Alzheimer's disease; AD, Alzheimer's disease; ELISA, enzyme-linked immunosorbent assay; APP, amyloid precursor protein; NFTs, neurofibrillary tangles; Tg, transgenic; PS1, presenilin 1; mAb, monoclonal antibody; Tricine, *N*-[2-hydroxy-1,1-bis(hydroxymethyl)ethyl]glycine; wt, wild type; NSP, non-spatial pre-training; PDAPP, APP transgenic mice constructed using the platelet derived growth factor beta promoter.

This paper is available on line at http://www.jbc.org

Downloaded from www.jbc.org at NATHAN S KLINE INSTITUTE, on December 6, 2012

ways, and in cases where this caveat does not apply, the transgenic animals may display only facets of the AD phenotype (16). With regard to neuropathology, the phenotypes created thus far include amyloid deposits that closely resemble those seen in AD, selective neuronal loss (in one instance), some hyperphosphorylation of tau, but no deposition of NFTs (17–20). Neuropathological abnormalities in singly transgenic mice may not appear until 6–9 months of age and may not be robust until animals are well in excess of 1 year of age (see "Discussion"). Other complications encountered in these models include hippocampal atrophy (21), neonatal lethality attributed to overexpression of APP (22, 23), and complex and variable relationships between cognitive dysfunction and transgene expression (18, 21, 23–25). Here we describe a new line of transgenic mice that exhibits deposition of Aβ-amyloid and robust cognitive deficits by the age of 3 months. These mice have a demonstrated utility for assessing procedures that interfere with amyloidogenesis (1) and may serve as a platform to create more sophisticated models of AD.

MATERIALS AND METHODS

Construction and Analysis of Tg Mice—The APP695 cDNA cassette was based upon an isolate of the cDNA clone described by Kang *et al.* (26). A *Sma*I to *Spe*I fragment including 90 and 269 base pairs of the wt APP cDNA 5′- and 3′-untranslated region was cloned into the plasmid vector pUC19 (27). This clone was subjected to mutagenesis using the "transformer" protocol (CLONTECH) to convert the 5′ *Sma*I site to a *Sal*I site, with a second *Sal*I site deriving from the pUC19 polylinker. The ~2.4-kilobase pair *Sal*I fragment was excised and inserted into the *Sal*I site of pBR322 (28), to exclude extraneous polylinker sites and thereby facilitate swapping of internal APP restriction fragments containing either Swedish (KM670/671NL) or Swedish plus Indiana (V717F) mutations ("Quick-change", Stratagene Inc.). Completed plasmids were sequenced in their entirety with a total of 12 sequencing primers covering the APP coding region, to exclude the possible presence of erroneous mutations either present in the starting plasmids or introduced during *in vitro* manipulations. *Sal*I fragments of APP or *Xho*I fragments of PS1 (9) were then cloned into cos.Tet (29). *Not*I transgene fragments excised from this cosmid vector were purified and injected into oocytes of different genetic backgrounds as noted, and founder animals were identified by dot-blot hybridization analysis of genomic DNA using a probe within the hamster PrP gene 3′-untranslated region as described previously (9, 30). Double transgenic mice deriving from crosses of transgene heterozygotes were identified by dot-blot hybridization analysis using human APP or PS1 cDNA probe fragments.

Protein Analysis—Western blots were performed by enhanced chemiluminescence as described previously (9), except ECL-Plus (Amersham Pharmacia Biotech) was used in conjunction with a "Storm" imaging system (Molecular Dynamics) for quantitative analyses. For ELISA analysis, C3H/B6 × FVB/N mice at 4, 6, 8, 10, and 26 weeks of age were transcardially perfused with cold saline. The entire brain was removed and snap-frozen until analysis. Cerebral Aβ was solubilized in a 5 M guanidine HCl, 50 mM Tris-HCl, pH 8.0 buffer (31), agitated, aliquoted, and stored at −80 °C. Thawed aliquots were diluted 10-fold or more and assessed for Aβ40 or Aβ42 using commercially available enzyme-linked immunosorbent assays (ELISAs) specific for either Aβ40 or Aβ42 and calibrated with synthetic Aβ peptides (BIOSOURCE International). The Aβ40 ELISA does not display any cross-reactivity with Aβ42 or Aβ43, and the Aβ42 ELISA does not react with either Aβ40 or Aβ43. Each brain was analyzed in duplicate or triplicate, with the average value reported for each brain.

Survival Census—All pups were weaned at an age between 21 and 24 days. The identification of pups genotypes was carried out between 23 and 26 days of age. Therefore, the reliable estimation of Tg mice survival is limited to their post-weaning age. Statistical analysis of survival as a function of genetic background was carried out on three cohorts of TgCRND8 mice as follows: (C57) × (C3H/C57), (FVB) × (C3H/C57), and (C3H/C57/129SvEv/Tac) × (129SvEv/Tac). For comparative purposes the survival of non-Tg littermates was included, and the analysis was performed for the 1st year of life. Since the mortality of non-Tg mice was minimal (1 non-Tg mouse out of the total of 158 included in the analysis died at the age of 26 days), non-Tg mice were pooled across their genetic backgrounds for graphical presentation and statistical analyses. The probability of survival was assessed by the Kaplan-Meier technique (32), computing the probability of survival at every occurrence of death, thus making it particularly suitable for small sample size cases with variable event intervals. The comparisons of cumulative survival curves for each genetic background of mice were performed using Tarone-Ware test, which weighs early events less than log rank or Breslow tests.

Histology and Immunohistochemistry—Mice were anesthetized and perfused with saline in accordance with The Canadian Council for Animal Care guidelines. Generally, brains were removed and bisected in the mid-sagittal plane. One-half was snap-frozen, and the portion for immunohistochemistry was fixed in 10% neutral buffered formalin for a minimum of 48 h. These specimens were then batch-processed on an automatic tissue processor overnight with vacuum on each station to aid penetration. Paraffin sections were cut at 5 microns and affixed to Fisher brand Superfrost/Plus slides to ensure adhesion. Sections were stained by Bielschowsky's silver impregnation, cresyl violet, thioflavine S, and Luxol Fast Blue combined with hematoxylin and eosin, as noted in the figure legends. For general morphological characteristics, 12 TgCRND8 mice from the hybrid C3H/B6 background, age 43–440 days, were studied. Additionally, 5 TgCRND8 mice (n = 2, 213 days; n = 3, 282 days) and 4 non-transgenic controls (n = 3, 213 days; n = 1, 282 days) were sectioned coronally to investigate hippocampal morphology. The percent volume occupied by the dorsal hippocampus within the surrounding brain regions was estimated using the Cavaleri point counting method. Paraffin-embedded brains were serially sectioned on a rotary microtome at a thickness of 10 μm (as described above) and stained with either hematoxylin and eosin or cresyl violet to delineate the hippocampal borders. The hippocampus was defined to include all regions of the hippocampus proper, hilus, and dentate gyrus. To represent the dorsal hippocampal region a total of 6 serial sections were collected for analysis (every 15th section, starting with the first section in which the hippocampus was visible). Brain sections were visualized using a video microscopy system (Zeiss Axoplan, using a lens for × 4 magnification) and a superimposed point grid (680 μm spacing). Points falling over the hemisphere and those falling over the hippocampus were tallied. Volumes were then estimated using the formula: $V = \Sigma_{\text{points}} \cdot$area per point$\cdot$section thickness$\cdot$section spacing. Student t tests were performed to compare mean volume data.

For immunohistochemistry, all sections were blocked in dilute (3%) hydrogen peroxide and non-immune goat serum. Epitope retrieval, in the form of a 5-min immersion in formic acid, was carried out prior to demonstration of amyloid and synaptophysin immuoreactivity. In all cases the primary antibody was left to react overnight at 4 °C. The remaining steps using the Dako StreptABC complex-horseradish peroxidase-conjugated "Duet" anti-mouse/rabbit antibody kit were completed according to the protocols provided by the manufacturer. End products were visualized with diaminobenzidine. Sections were lightly counterstained with hematoxylin and were resin-mounted. The sources of the antibodies used were as follows: 369 from Sam Gandy; 4G8 *versus* Aβ residues 17–24 from Richard Rubenstein; Aβ42, 3542 from Frédéric Checler; 6F/3D *versus* Aβ residues 8–17, synaptophysin, and anti-ubiquitin from Dako Inc.; 6E10 *versus* Aβ residues 1–16 from Senetek Inc.; glial fibrillary acidic protein monoclonal from Roche Molecular Biochemicals; NF200 from Novo Castra Laboratories; CD11b from Chemicon Labs; and hyperphosphorylated tau, AT8, from Innogenetics, Gent, Belgium. The 6F/3D antibody was of particular use for quantitative studies using image analysis software as it visualized structures (*i.e.* dense-cored plaques) with sharp boundaries.

Behavioral Tests and Data Analysis—Experimentally naive TgCRND8 mice were tested at 11 weeks of age in two cohorts (N_{Tg} = 10, $N_{\text{non-Tg}}$ = 7 in total) in the reference memory version of Morris water maze test. The water maze apparatus, mouse handling, and general testing procedure are described elsewhere (1, 33). Prior to the spatial learning training, all mice underwent non-spatial pre-training (NSP), to assess swimming abilities and familiarize mice with the test (1). Two days following the NSP phase, all mice underwent a reference memory training with a hidden platform placed in the center of one quadrant of the pool (northeast) for 5 days, with 4 trials per day. After the last trial of day 5, the platform was removed from the pool and each mouse received one 60-s swim "probe trial." Escape latency (in seconds), length of swim path (centimeter) and swim speed (cm/s), were recorded using an on-line HVS image video tracking system (33). For the probe trials, an annulus crossing index was calculated, which represents the number of passes over the platform site minus the mean of passes over alternative sites in other quadrants. The index expresses the spatial place preference and controls for alternative search strategies without place preferences, such as circular search (34, 35). Behavioral data was analyzed using a mixed model of factorial analysis of variance. Degrees of

Downloaded from www.jbc.org at NATHAN S KLINE INSTITUTE, on December 6, 2012

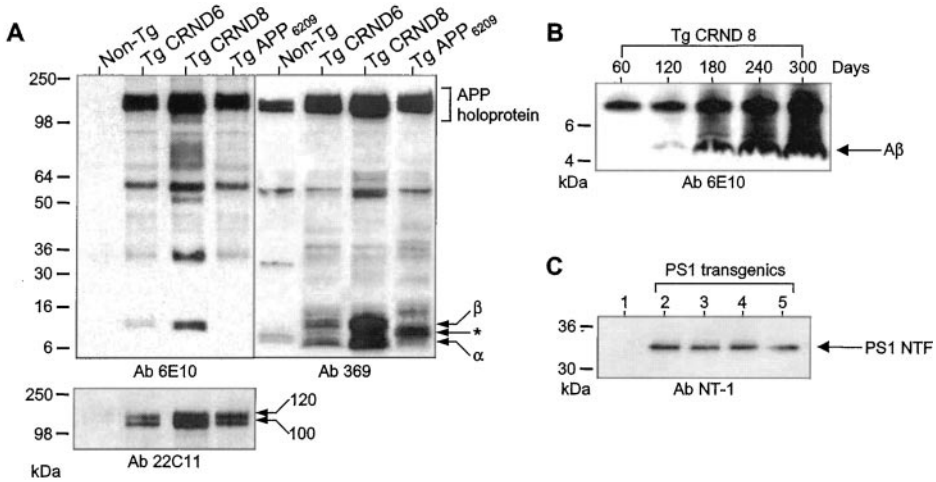

FIG. 1. **Western blot analysis of transgene expression.** 10% brain homogenates made in 0.32 M sucrose were diluted with Laemmli buffer, sonicated, and run on 10–20% Tricine gradient gels (NOVEX). Following transfer to nitrocellulose, human APP and PS1 were detected using C- and N-terminal-specific mAbs and developed by ECL (Amersham Pharmacia Biotech). *A,* comparison of APP expression levels in Tg lines. *1st lane,* Non-Tg; *2nd lane*, Tg CRND6; *3rd lane*, Tg CRND8; and *4th lane*, Tg APP6209. Proteins were detected with human APP-specific C-terminal mAb 6E10 (*left panel*), C-terminal antibody 369 reactive against mouse and human APP (*right panel*), and N-terminal antibody 22C11, also reactive against mouse and human APP (*lower panel*). Positions of high molecular weight APP holoprotein and holoprotein derivatives ("APP holoprotein"), and C-terminal stubs are indicated. *B,* time course of Aβ accumulation in Tg CRND8 mice: *1st lane,* 60 days; *2nd lane*, 120 days; *3rd lane,* 180 days; *4th lane*, 240 days; and *5th lane*, 300 days. Detected with human-specific APP C-terminal mAb 6E10. *C,* comparison of protein expression levels in Tg mice expressing single and double mutants of PS1. Normalized samples of brain homogenates are presented. Detection is with the human-specific PS1 N-terminal mAb NT-1 (72). *Lane 1,* Non-Tg; *lane 2*, TgPS1(L286V)1274; *lane 3*, TgPS1(WT)1098; and *lanes 4* and *5* represent samples from TgPS1(L286V+M146L)6500 mice.

freedom were adjusted by Greenhouse-Geisser epsilon correction for heterogeneity of variance.

RESULTS

Creation of TgCRND8 Mice Expressing Mutant APP

Previous experiments have indicated that overexpression of APP above a threshold of ~4× endogenous is a prerequisite for deposition of amyloid plaques in the central nervous system (18, 22). To avoid the toxic effects associated with these levels of APP overexpression (22, 23, 36, 37), we exploited (i) permissive strain backgrounds and (ii) APP cassettes, including multiple mutations, to maximize production of Aβ for a given level of APP expression. Transgene constructs were based upon a cDNA cassette encoding the major APP isoform in human brain, APP695. This cassette was modified to include either one or two FAD mutations: the "Swedish" mutation (K670N, M671L) and the "Indiana" mutation (V717F), lying adjacent to the N- and C-terminal boundaries of the APP Aβ domain, respectively. APPSwe and APPSwe+717 cDNAs were introduced into cos.Tet (29), a cosmid-based expression vector derived from the Syrian hamster prion protein gene. This vector directs position-independent transgene expression in central nervous system neurons and, to a much lesser extent, astrocytes (38–41). Microinjections into C3H/HeJ × C57BL/6J or (C3H/HeJ × C57BL/6J) × C57BL/6J oocytes (the strains are hereafter referred to as C57 and C3H) yielded a number of putative founders but just two stable transgenic lines designated Tg CRND6 and TgCRND8. These lines harbor APPSwe and APPSwe+V717F transgenes, respectively.

Expression of APP and Aβ Peptide in TgCRND8 Mice

APP-specific antibodies were used to establish transgene expression from founder lines, with previously characterized TgAPPwt6209 transgenic mice providing a point of reference (22). Use of the N-terminal antibody 22C11, which reacts with mouse and human APP, demonstrated overexpression of the full-length mature form of APP of ~120 kDa and different lower molecular mass species of 100 kDa (which are not resolved in this gel system), including immature APP, and APP cleaved at the α- and β-secretase sites, $APP_{S\alpha}$ and $APP_{S\beta}$ (Fig. 1*A*). Overexpression in the TgCRND8 line relative to mouse APP holoprotein detected in non-Tg controls was estimated by quantitative image analysis at ~5-fold. Similar results for high molecular weight APP species were obtained with antibody 369, which reacts with an epitope close to the C terminus of APP shared by mouse and human APP (Fig. 1*A*). Lower molecular weight species deriving from APP processing were also observed in brain extracts of TgCRND8 and TgCRND6 mice analyzed with the human APP-specific monoclonal antibody 6E10 antiserum (epitope positioned N-terminal to the α-secretase cleavage site) and antibody 369. These polypeptides represent APP C-terminal stubs arising from cleavage at the α- and β-secretase sites, with antibody 369 recognizing both species and antibody 6E10 recognizing only the longer β-stubs. As anticipated, the APP6209 Tg line encoding wt human APP does not exhibit β-stubs (as it lacks the Swedish mutation that favors cleavage at this position) but exhibits α-stubs with a reduced electrophoretic mobility due to the inclusion of a c-Myc epitope tag within the C terminus of the APP cDNA cassette (22).

In TgCRND8 mice, increasing levels of a 4-kDa species (but not β-stubs) were detected by Western blot analysis as the animals aged (Fig. 1*B*). To investigate the composition of these 4-kDa Aβ peptide species, we performed ELISAs specific for Aβ40 and Aβ42. Both human Aβ40 and Aβ42 were detected in the brains of Tg CRND8 mice. No signals above background were detected in non-Tg animals. Levels of both peptides increased with age, although in different fashions (Table I). Thus Aβ40 levels were stable between 4 and 10 weeks of age. Aβ42 increased slowly between 4 and 8 weeks, with a potent increase at age 10 weeks, such that it predominated over Aβ40 by a ratio of ~5:1. There was considerable spread in Aβ40 and Aβ42 levels in 10-week-old mice, with levels of Aβ40 varying from 25 to 234 ng/g of brain and Aβ42 ranging from 115 to 728 ng/g of brain. The increase in Aβ42 and the sample-to-sample variation between mice at age 10 weeks likely represents a transition point as Aβ42, first present in soluble form, begins to assemble into insoluble amyloid deposits. Measured at 6 months of age, levels of both Aβ42 and Aβ40 were enormously

Downloaded from www.jbc.org at NATHAN S KLINE INSTITUTE, on December 6, 2012

TABLE I
Aβ peptide species in young TgCRND8 mice

Age	Gender[a]	Aβ42[b]		Aβ40[b]		Aβ42/Aβ40
		Mean ± S.D.	Range	Mean ± S.D.	Range	Mean ± S.D.
weeks						
4	3F, 3M	40.9 ± 4.1	35–46	55.2 ± 3.6	49–60	0.74 ± 0.04
6	4F, 3M	55.3 ± 6.9	47–63	61.3 ± 11.4	48–82	0.93 ± 0.19
8	4F, 3M	96.9 ± 56.3	59–215	55.8 ± 4.8	46–63	1.07 ± 0.83
10	9F, 1M	298.1 ± 209.9	115–728	69.5 ± 61.1	25–234	5.06 ± 1.56
26	5M	20,783 ± 6599	12,476–29,260	10,584 ± 1495	9,262–13,157	1.96 ± 0.59

[a] Using unpaired *t* tests, the levels of Aβ40 and Aβ42 were not found to differ between males and females, from 4 to 8 weeks of age.
[b] Values are expressed as nanograms of peptide per g of brain (wet weight) derived from duplicate or triplicate determinations of each animal.

increased and were ~510 and 190 times, respectively, the levels observed in 4-week-old mice (which are free of amyloid plaque deposits; Fig. 5*A*).

Postnatal Lethality in TgCRND8 Mice

To gain insight into the ability of genetic backgrounds to modulate lethality associated with APP overexpression (and, from a practical point of view, to preempt premature extinction), the newly established TgCRND8 line was bred to different strain backgrounds. Progeny of an F1 cross to the C3H/HeJ ("C3H") strain were bred to mice derived from FVB/N and 129SvEv/Tac backgrounds. Estimated Kaplan-Meier cumulative survival curves for TgCRND8 mice and their littermates during post-natal development are presented in Fig. 2. Inspection of the curves clearly indicates improved survival of mice with the APP transgene expressed on the (C57) × (C3H/C57) genetic background. In this cohort of Tg mice ($n = 52$), 20 mice died before the age of 120 days, decreasing their survival to 60% and with three deaths at 130 days and three further deaths after 250 days. When the APP transgene was expressed on either (C3H/C57/129SvEv/Tac) × (129SvEv/Tac) or (FVB) × (C3H/C57) genetic backgrounds ($n = 12$ and $n = 41$ respectively), survival dropped rapidly to 25–40% within the first 120 days of their post-natal life (Fig. 2). After this time point, survival with the (C3H/C57/129SvEv/Tac) × (129SvEv/Tac) genetic background dropped slightly to 33% (one death at 159 days) with only 25% (3 mice) of the cohort surviving until 365 days. Similarly, the survival of the TgCRND8 mice with (FVB)×(C3H/C57) background dropped rapidly within the first 120 days of post-natal age (Fig. 2) with 17% of mice ($n = 7$) surviving until 365 days of age. The survival of mice with the (C57) × (C3H/C57) was significantly better than survival of Tg mice with (FVB) × (C3H/C57) or (C3H/C57/129SvEv/Tac) × (129SvEv/Tac) backgrounds (Tarone-Ware statistics: 5.13, $p < 0.05$, and 19.01, $p < 0.001$, respectively). The survival curves of the latter two genetic backgrounds did not differ significantly from each other (Tarone-Ware statistics: 0.42, $p > 0.05$), and the survival of TgCRND8 mice with the three genetic backgrounds was significantly different from the survival of non-Tg littermates (Tarone-Ware statistics >50, all p values < 0.001.

Although these data suggest significantly increased mortality of TgCRND8 mice as a consequence of a genetic contribution of 129SvEv/Tac or FVB mouse strains, some caveats have to be taken into consideration. First, the relatively small sample sizes of the studied cohorts, especially with the 129SvEv/Tac strain, where only a few mice survived for a long period, may not reliably reflect survival rates at later stages of life. The comparisons of larger cohorts should provide better estimation of survival curves. Second, future survival censuses must be extended to the pre-weaning developmental stage. The selective survival of pups before weaning, or for that matter at the pre-natal stage of development, may cause a bias of a particular cohort entering post-weaning stage. Also, the genetic composition of the particular outbred TgCRND8 parent might be a greater contributor to the differences in survival among the crosses than the composition of the inbred parent. Nonetheless, the major finding of the survival analysis, that the (C57) × (C3H/C57) genetic background significantly reduces mortality in TgCRND8 mice, is in accord with our starting hypothesis. Fifty percent of the studied cohort of 52 mice survived for a year with minimal mortality observed after the first 3 months of age. As shown in previous investigations, the cause of post-natal lethality was not obvious (22). No overt changes were revealed by routine histopathology, although it should be noted that seizures were observed in a small fraction of TgCRND8 animals, and APP transgenes have been correlated with altered vascular responses (37).

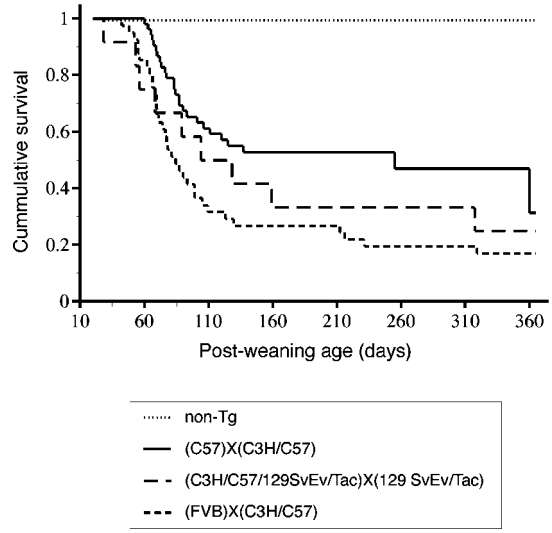

FIG. 2. **Cumulative survival curves (Kaplan-Meier survival analysis) of TgCRND8 mice in different genetic backgrounds.** Cumulative survival curves of TgCRND8 mice as a function of the transgene genetic background. The survival of Tg mice on the (C57) × (C3H/C57) genetic background ($n = 52$) was the highest, with 50% of mice surviving until 365 days of age (upper cut-off of the analysis). In contrast, the survival of the Tg mice on (C3H/C57/129SvEv/Tac) × (129SvEv/Tac) and (FVB)×(C3H/C57) backgrounds ($n = 12$ and $n = 41$ respectively) was affected by increased mortality within the first 120 days of their post-natal age. In the case of Tg mice with the (C3H/C57/129SvEv/Tac) × (129SvEv/Tac) genetic background, only 3 (25%) out of 12 mice survived until the age of 365 days, and only 17% (7 out of 41) of the (FVB) × (C3H/C57) Tg mice reached the age of 365 days.

Cognitive Changes in TgCRND8 Mice

Non-spatial Pre-training—Partial results related to the impaired acquisition of spatial information, as measured by the escape latency, were reported previously for a small cohort of mice (1). Here we present a characterization of a larger cohort of mice, and we include their behavioral analysis during NSP. The analysis showed that during NSP at age 10.5 weeks TgCRND8 mice performed comparably to non-Tg littermates when randomly searching the pool for a hidden platform. Escape latencies and lengths of search paths in the last trial of

Downloaded from www.jbc.org at NATHAN S KLINE INSTITUTE, on December 6, 2012

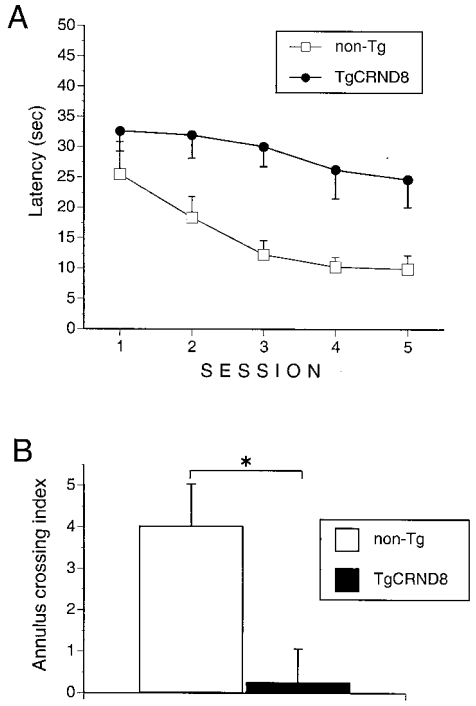

FIG. 3. **Reference memory version of Morris water maze test in TgCRND8 mice.** *A,* at 11 weeks of age, experimentally naive TgCRND8 mice (N_{Tg} = 10) show significant impairment in the acquisition of the spatial information relative to their non-Tg littermates ($N_{non\text{-}Tg}$ = 7). *B,* represents an annulus crossing index (the number of passes over the platform site in TQ, minus the mean of passes over alternative sites in other quadrants) during the probe trial administered after the last training trial of day 5. A positive index indicates selective focal search of the previous platform position, an index approximating zero reflects non-spatial or circular search of the pool. The TgCRND8 mice showed a significantly impaired ($p < 0.01$) spatial bias for the platform position as compared with their non-Tg littermates. *, $p < 0.01$. *Vertical bars* represent S.E.

NSP for the groups were not significantly different (50.0 ± 7.3 *versus* 57.6 ± 8.8 s for latency and 961.1 ± 165.0 *versus* 1351 ± 247.4 cm for path-length, for the non-Tg and Tg mice, respectively). A "visible platform trial" administered during NSP, where the position of the submerged platform was marked by a striped beacon, also failed to reveal differences in performance between non-Tg and Tg groups. Average latencies to reach the cued platform were 9.9 ± 2.0 and 9.1 ± 1.6 s for non-Tg and Tg mice, respectively. The swim paths were 167.3 ± 16.1 cm for non-Tg and 153.1 ± 14.2 cm for Tg mice, and both groups had comparable swim speeds of 21.6 ± 1.4 and 20.2 ± 1.7 cm/s for non-Tg and Tg mice, respectively. In conclusion, these analyses showed TgCRND8 mice performed a random search comparable to non-Tg littermates when presented with the submerged platform and had similar swim paths to a visible platform when extra-maze distal spatial cues were occluded by a curtain.

Water Maze, Reference Memory Test—TgCRND8 mice at 11 weeks showed impairment in the acquisition of spatial information during place discrimination training. They had significantly longer escape latencies to reach the escape platform (Fig. 3*A*; $F(1,15) = 17.98$, $p < 0.001$) and longer search paths ($F(1,15) = 15.91$, $p < 0.001$). Both, Tg and non-Tg groups significantly improved during training ($F(4,60) = 3.29$, $p < 0.02$; $F(4,60) = 3.33$, $p < 0.02$, the latency and path, respectively), and no significant interaction between the groups and sessions was found in both measures. The concordance between measures of latency and search path is not surprising, because the TgCRND8 mice did not differ significantly from the non-Tg littermates in their swim speed during the test ($F(1,15) = 2.53$, $p > 0.05$). The pronounced spatial learning impairment of Tg mice was confirmed during the probe trial administered after the completion of training. They showed lower ($t(15) = 2.99$, $p = 0.01$) annulus crossing index (Fig. 3*B*), searching the pool in a circular fashion and frequently crossing the centers of alternative quadrants (with an annulus crossing index approaching a zero value).

Neuropathology in TgCRND8 Mice

TgCRND6 mice expressing the Swedish mutant form of APP (see Fig. 1) on a B6 × C3H background failed to exhibit cerebral amyloid at ages up to 450 days. Similar results were obtained for two other Tg lines resulting from the microinjection of the same DNA construct into a FVB/N × 129SvEv/Tac background (not shown). On the other hand, hemizygous TgCRND8 mice expressing the double mutant form of APP exhibited potent deposition of cerebral amyloid, present in all animals by 90 days of age. In contrast to PDAPP mice expressing a V717F APP transgene (21), no difference in the volume of the dorsal hippocampus (or in the surrounding regions) was detected between Tg and non-Tg mice ($p < 0.05$ for all values). In TgCRND8 mice, the dorsal hippocampus occupied ~11.0 ± 0.3% of the volume of coronal sections (means ± S.E. of the mean), whereas in the non-Tg mice this value was 10.3 ± 0.2%. Also, the neuronal cytoarchitecture of the TgCRND8 mice appeared normal.

Amyloid deposits in TgCRND8 mice were successfully stained with Aβ42-specific antibodies, as anticipated from prior studies of the mechanism of action of the V717F mutation (5). In addition to confirming dense-cored deposits in aged TgCRND8 mice, the human APP-specific monoclonal antibody 4G8, and to a lesser extent monoclonal antibody 6F/3D, also detected diffuse immuno-staining in the neuropil (using formic acid-treated sections: Fig. 4*B*). These findings were compatible with both the previously described specificity of the 4G8 antibody (42, 43), and the propensity of other mice expressing APP codon 717 mutations to generate "diffuse" amyloid deposits (19, 21, 23). Although human APP was also expressed systemically in TgCRND8 mice, in accord with the tropism of the PrP gene promoter (44), amyloid deposits were not apparent by immunostaining in the kidney, lung, skeletal, and cardiac muscle of aged animals (not shown). These observations suggest a role for tissue-specific factors affecting amyloid deposition and/or APP processing.

Plaque Ontogeny—A single plaque was noted in one TgCRND8 animal at 43 days. Plaque load increased with age and spread to more regions of the brain such that multiple plaque deposits were present per sagittal section in most mice at 65 days of age, and in all mice by 90 days of age. Although studies on large cohorts of mice are in progress, analyses of representative mice revealed between 11–35 and 22–43 plaques in a mid-sagittal section of the cortex at the ages of 90 and 150 days, whereas burdens were greatly increased at 240 and 350 days of age (127–416 and 528–1024 plaques, respectively). A similar pattern of increase pertained to the hippocampal formation with 1–5 and 11–12 plaques at 90 and 150 days and 39–65 and 123–147 plaques at 240 and 360 days, respectively. Thus, the time period for a rapid increase in amyloid burden assessed histologically lags slightly behind that determined biochemically by ELISA assays (Table I).

Plaque Distribution—The plaque present at 43 days was located in the subiculum. The frontal cortex of TgCRND8 mice often had several plaques by 65 days, whereas plaques were rare or absent in the white matter tracts (corpus callosum and alveus) and CA1 region of the hippocampus at this time. By 101 days plaques were widespread in many regions of the cortex as well as in the hippocampus proper, the dentate gyrus, the

Downloaded from www.jbc.org at NATHAN S KLINE INSTITUTE, on December 6, 2012

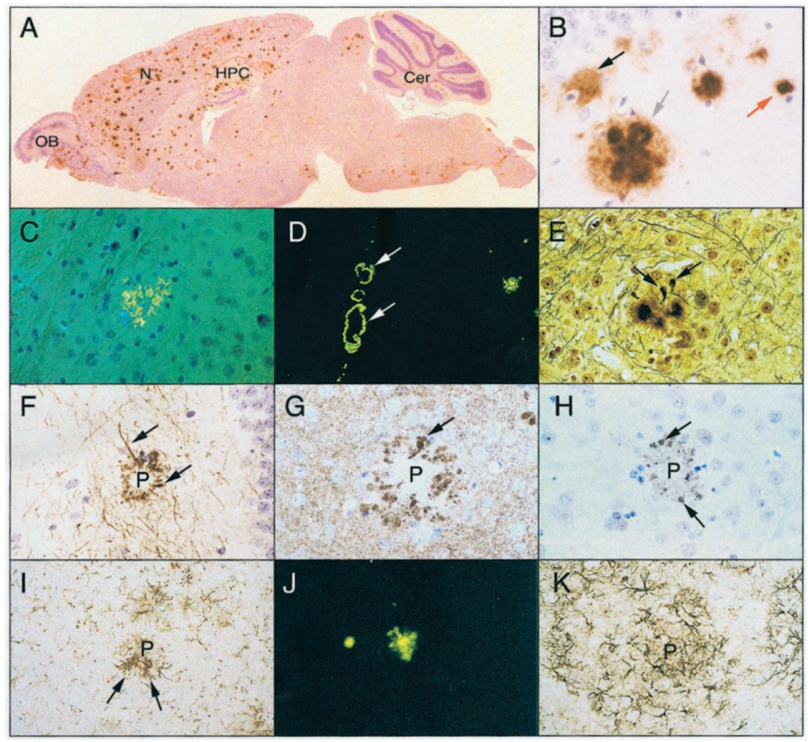

FIG. 4. **Properties of amyloid deposits from TgCRND8 mice.** *A,* sagittal section of an 8-month-old TgCRND8 mouse immunostained with 4G8 anti-Aβ antibody: *Cer*, cerebellum; *HPC*, hippocampus; *N*, neocortex; *OB*, olfactory bulb. *B,* dentate gyrus (× 400 magnification) in a 12-month-old TgCRND8 mouse immunostained with 6F/3D antibody and illustrating different varieties of amyloid deposits: dense-cored (*red arrow*), multicored (*gray arrow*), and diffuse (*black arrow*). *C–K* illustrate the tinctorial and immunostaining profiles of amyloid deposits in a 5.5-month-old TgCRND8 mice (× 400 magnification). *C,* staining with Congo Red showed typical *apple green* and *orange* birefringence with a polarized light source. *D,* perivascular amyloid stained with thioflavine S (*white arrows*). Bielschowsky stain (*E*) and NF-200 (*F*) reveal dystrophic neurites (*arrows*) adjacent to plaques (*P*). *G* and *H* represent synaptophysin and ubiquitin-positive structures in the periphery of plaque deposits, indicative of dystrophic buttons. *I–K* illustrate focal inflammatory responses. *I,* anti-CD11b antibody, *J,* thioflavine S stain of an adjacent section, and *K,* GFAP staining of a third adjacent section.

olfactory bulb, and within the pial vessels. The thalamus (111 days), then the cerebral vasculature and striatum (196 days), followed by the cerebellum and brain stem (243 days) all became progressively burdened by plaques. This pattern of deposition, with cortex and hippocampus affected early on and the cerebellum spared until a late stage in disease, is similar to that seen in AD (45).

Plaque Morphology—The first plaques observed were small, cored deposits, with no radiating amyloid surrounding them (65 days). By 101 days, the plaques varied in size, with some larger plaques having haloes of radiating amyloid. By 131 days the plaques became more heterogeneous in nature. Plaques varied greatly in size as the age of the mice increased, with some being multicored in older animals. Diffuse amyloid deposits appeared in the olfactory bulb at an early stage (101 days). However, outside of the olfactory bulb, diffuse amyloid (*i.e.* amyloid not obviously associated with a cored plaque) did not appear until 243 days, as detected with the 6F/3D antibody. Diffuse amyloid was found primarily in the caudate, cerebellum, and molecular layer of the dentate gyrus (all at 243 days). By 315 days diffuse amyloid appeared throughout the cortex (see Fig. 4*B*).

The majority of amyloid plaque deposits in TgCRND8 mice, including those first to appear at 65 days, stained positive for thioflavine S. These early deposits also revealed Congo Red birefringence. Together these data indicate the deposited amyloid peptide adopts a β-sheet conformation. Amyloid plaques in TgCRND8 mice were associated with dystrophic neurites, as indicated by a variety of histochemical and immunohistochemical stains (Fig. 4). For example, Bielschowsky silver impregnation revealed dystrophic neuritic processes around plaque cores (Fig. 4*E*). Similar structures were imaged by antibodies raised against the 200-kDa isoform of neurofilament (NF-200; Fig. 4*F*), synaptophysin (Fig. 4*G*), and ubiquitin (Fig. 4*H*). The first enlarged plaque-associated neurites were seen with Bielschowsky, synaptophysin, and NF-200 staining at 111 days of age. Dystrophic pathology became more evident as the mice aged further and the frequency of large, dense-cored plaques increased. Finally, it was noteworthy that dystrophic neurites were only observed in the immediate vicinity of plaques, indicating these structures are a direct consequence of amyloid deposition in the TgCRND8 mice.

Neuroinflammation—Mature plaques in TgCRND8 mice were associated with a focal inflammatory response. Elongated cells in periphery of dense-cored amyloid deposits visualized by Luxol fast blue staining or focal staining with a *Griffonia simplicifolia* lectin I isolectin B4 stain (not presented) and staining with anti-CD11b antibody probe (Fig. 4*I*) were consistent with the presence of microglial cells. This microglial activation was accompanied by intense local astrocytic gliosis, illustrated by GFAP staining of adjacent sections encompassing a thioflavin-positive plaque (Fig. 4, *K* and *J*). This astrocytic response clearly exceeded a low basal level of staining of GFAP-positive astrocytes (mostly evident within white matter tracts) noted in both transgenic and non-transgenic mice.

Acceleration of Amyloid Deposition by Co-expression of Presenilin-1 Transgenes

Amyloid deposition in TgCRND8 mice was enhanced by mutant human PS1 transgenes co-expressed with human APP via usage of the same cos.Tet transgene vector (Fig. 5, *right-hand panels*). This effect was evident in terms of a potent increment in plaque burden over age-matched TgCRND8 single transgenic controls. Conversely, expression of wt human PS1 had no overt effect upon amyloid burden (not shown). With a PS1 transgene incorporating two FAD mutations in *cis* (M146L and L286V (46)), the potentiation was particularly remarkable. Here there was robust deposition of plaques by 30–45 days of age (33 days of age presented in Fig. 5*B*). Notably, the graded effects observed for wild type, single, and double mutant transgenes upon amyloid deposition cannot be attributed to different PS1 expression levels, as these were very closely matched between the three selected TgPS1 lines (wild type, mutant, and double mutant, Fig. 1*C*).

DISCUSSION

Factors Affecting APP Transgenesis—Although transgenesis is generally regarded as a routine technique, the APP gene,

Downloaded from www.jbc.org at NATHAN S KLINE INSTITUTE, on December 6, 2012

first cloned over a decade ago, can be seen to present particular challenges. Difficulties encountered thus far include low expression levels in first generation Tg mice, neonatal lethality associated with high level expression in second generation mice, and physiological endoproteolysis to generate multiple subfragments with diverse biological activities, some of which (*e.g.* neuroprotection (reviewed in Ref. 47) may confound the study of neuropathogenesis. We modified a number of parameters in our experimental design in an effort to reduce the "noise" from these confounding effects and thereby facilitate study of the pathogenic attributes of the Aβ peptide; such pathogenic attributes are clearly suggested by genetic, neuropathological, and toxicological studies (12–14, 48). Our strategy involved using the following: (i) an expression cassette that retained ~90 nucleotides of the APP mRNA 5′-untranslated region adjacent to the start codon, as APP is expressed at high levels for a single copy gene and likely already contains optimized translational initiation signals; (ii) a prion protein cosmid vector that can drive high level pan-neuronal expression in the central nervous system; (iii) two pro-endoproteolytic FAD mutations, to obtain a high level of Aβ peptide for a given level of APP expression; and (iv) use of a genetic background that may offer a degree of protection against high level APP expression favored by parameters i and ii.

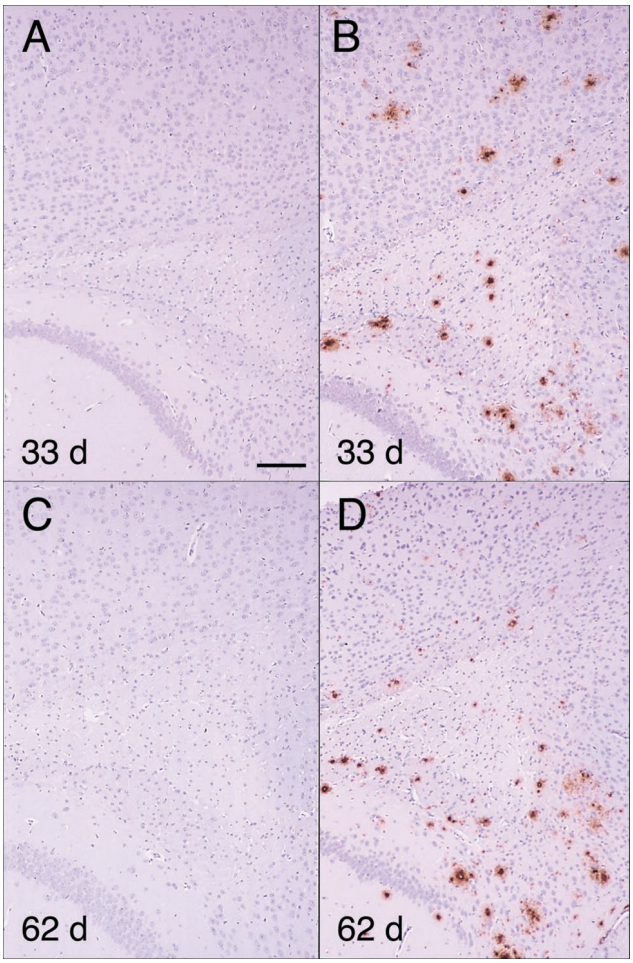

FIG. 5. **Aβ-containing plaques in the cortex of single and double transgenic mice.** Panels show sagittal sections of the neocortex adjacent to the hippocampus. *Left-hand panels* (*A* and *C*) depict "single" transgenic TgCRND8 mice. *Right-hand panels* (*B* and *D*) depict "double" transgenic TgCRND8 mice co-expressing either human presenilin 1 (*B,* TgPS1(M146L+L286V)6500; *D*, TgPS1(L286V)1274). Each *horizontal row* represents single and double -Tg littermates at the same age: *A* and *B*, 33 days; *C* and *D*, 62 days. Immunohistochemical analyses presented were obtained with the 4G8 monoclonal antibody. Note enhanced plaque deposition in double Tg animals. × 400 magnification.

It is possible that genetic background may have been important for establishing the TgCRND8 line. Our strategy was based upon the hypothesis that dominant alleles protective against APP overexpression present in the C3H background (36) would facilitate the establishment of Tg lines with high levels of expression. As injections into C3H oocytes are not usually attempted, the TgCRND8 line was established in an outbred C3H/B6 background. Survival curves presented here document that in TgCRND8 mice high levels of Aβ peptide and modest levels of APP α- and β-stubs can be tolerated in a C3H/B6 genetic background without grossly compromising viability (Fig. 2). Whereas these data are in accord with the starting hypothesis, they are incompatible with facile genetic analysis, as confounding effects due to independent segregation of alleles from the C3H and B6 strains conferring protection or sensitivity to APP overexpression cannot be excluded. Experiments to establish C3H congenic lines of TgCRND8 mice will lead to more definitive information on this point. Furthermore, it is of interest to note that the KM670/NL671+V717F construct injected into oocytes from another potentially protective genetic background (129SvEvTac × FVB/N (36)) yielded a transgenic line designated Tg19959, which also exhibits cerebral plaques at 3 months of age (data not shown). In sum, our results suggest manipulation of genetic background may reduce postnatal death associated with APP overexpression and should be considered in strategies for APP transgenesis. However, insofar as parameters i–iv have been used individually in the creation of APP Tg mice (8, 17–19, 22, 23), it is plausible that a synergism between all four parameters contributes to the desirable properties of TgCRND8 mice.

Biochemistry of TgCRND8 Mice—With the possible exception of the Tg19959 line, TgCRND8 mice are currently unique

TABLE II
Amyloid deposition in APP transgenic mice

Tg line	Aβ42 pmol/g[a]	Aβ40	Aβ42/40	Plaque onset	Ref.
	age months[b]	*pmol/g*[c]		*months*	
PDAPP	615 ± 333 (12)	~79[c]	~7.8	6–9	17
Tg2576	175 ± 26 (11–13)	264 ± 38	0.7	9	18
TgAPP/V717I[d]	~170 (15)	~440	~0.4	13	73
TgCRND8	4,600 ± 1,560 (6)	2,440 ± 350	2.0	3	This paper, (1)
	3200 ± 350[e] (6)	920 ± 125	3.5		

[a] Results of Aβ ELISAs are expressed per g (wet weight of brain). Transgenic mice are listed chronologically. Some values derive from formic acid extraction, whereas others use a guanidinium-hydrochloride procedure. Some values were converted from ng to g using values of 4328 and 4513 Da for Aβ 40 and 42, respectively.

[b] Except for the TgAPP/V717I line, all Aβ values are reported for a time point 3 months after the first onset of plaque deposition, as determined histologically. These time points are given in months (in parentheses).

[c] Aβ40 was calculated by subtraction of Aβ42 from total Aβ values.

[d] ELISA values represent plaque-associated (insoluble) Aβ.

[e] Second set of ELISA values derive from a control group of TgCRND8 mice immunized with islet-associated polypeptide (1).

Downloaded from www.jbc.org at NATHAN S KLINE INSTITUTE, on December 6, 2012

among single transgenic APP mice with regard to the severity of Aβ deposition. Histological deposition of Aβ in amyloid plaques in TgCRND8 mice is evident in 100% of animals by 3 months after birth (n = 28), earlier than in APP transgenic lines described previously (17–19, 49). These results find a parallel in measurements of Aβ40 and Aβ42 derived from ELISA assays (Tables I and II); for example, levels of Aβ42 in 6-month-old TgCRND8 mice approximate those seen in PDAPP mice at 16 months of age (31). Furthermore, two results emerging from these ELISAs show a direct parallel to AD pathogenesis and bear particular emphasis. First, the levels of total Aβ in TgCRND8 mice at 6 months of age, 3,200–4,600 pmol/g brain (as determined by two independent ELISA configurations employing different antibodies), fall into the range observed for sporadic AD cases, 500–5000 pmol/g wet tissue (50). Second, the ratio of Aβ42 to Aβ40 exceeds unity, as is also the case in sporadic AD (50) (and in PDAPP mice expressing a V717F mutation (31)). Insofar as Aβ42 is thought to be the most aggregation-prone and toxic form of Aβ, the skew toward the production of Aβ42 apparent in these mice presumably contributes to the unusually early onset of amyloid deposition.

Although the combined effect of the two FAD mutations affecting both β- and γ-secretase processing of APP is presumed to be a powerful determinant of this potent amyloidogenesis, it is notable that other "double mutant" TgAPP mice only show 100% of animals positive for plaques at 8–10, 18, or 21–25 months of age (19, 49, 51). Although the degree of APP overexpression could also prove crucial in distinguishing TgCRND8 mice from other double mutant TgAPP lines, further variables include PrP, *thy-1,* or platelet-derived growth factor-β promoters with different tropisms and different APP coding region cassettes (APP695, APP751, or intron-containing cassettes capable of producing all three APP isoforms).

Finally, it is remarkable that even though TgCRND8 mice exhibit a high basal synthesis of Aβ, levels of this peptide can be elevated to yet higher levels by mutant versions of PS1. Importantly, two PS1 mutations in *cis* shown to act in an additive way in transfected cells (46) behave in a similar fashion *in vivo*. Thus, double transgenic mice incorporating 4 FAD mutations can develop Aβ deposits by 1 month of age (Fig. 5*B*).

Neuropathology in Transgenic Models of Alzheimer's Disease—TgCRND8 mice exhibit AD-like amyloid plaque deposits with a variety of morphologies. Dense-cored deposits are present from an early stage, and the majority of these (>80%) can be stained with either Congo Red or thioflavine S. With aging, the plaques become larger and multicentric dense-cored deposits appear. Diffuse Aβ immunostaining is also apparent at later stages, being particularly prominent after formic acid pretreatment. Diffuse staining is evident as a penumbra around large plaques and also in the form of isolated deposits (*i.e.* not obviously associated with plaques) throughout the neuropil. From 5 months of age the mature plaques in TgCRND8 mice exhibit neuritic changes strikingly similar to those seen in AD (Fig. 4). Dystrophic neurites are revealed by silver impregnation or NF-200 immunostaining, with dystrophic boutons visualized by synaptophysin or ubiquitin antibodies. Astrocytes and microglial cells often encircle dense-cored deposits, indicating the plaques are capable of initiating an inflammatory response. The other pathological hallmarks of AD are generally accepted to include neuronal loss and the accumulation of NFTs. Focal neuronal loss has been reported in only one Tg model of AD (20, 52, 53), and analogous studies in TgCRND8 mice are underway. NFTs are absent in TgCRND8 mice, as indeed they are in other TgAPP mice. It is possible coding sequence divergence between mouse and human may be of importance, and expression of human tau and cognate tau kinases, perhaps the p25 fragment of p35 (54, 55) or glycogen synthese kinase 3β, may be required to fully recapitulate this pathology.

The Origins of Cognitive Dysfunction in Alzheimer's Disease—In Alzheimer's disease patients, pathological changes detected post-mortem are foreshadowed in the clinical presentation by erosion of mental function leading to frank dementia. Therefore, plausible animal models of AD should develop cognitive deficits at least by the time of appearance of AD-related neuropathology. TgCRND8 mice fulfill this expectation. They represent an example of mice expressing full-length APP where deficits in acquisition of spatial reference memory are present at the onset of AD-related neuropathology (Fig. 3) (1) and thus exhibit some similarities to Tg2576 mice (18, 24). In studies of other TgAPP mice, impaired performance in the water maze test preceded neuropathological changes (23) or was not reported (19). Impaired performance in other testing paradigms has been reported in PDAPP V717F mice, but here a subset of cognitive deficits was better correlated to confounding neuroanatomical abnormalities than to AD-related pathologies (21, 25). In the most recent studies, an age-related deficit in learning capacity was detected in PDAPP mice using a new water maze testing regimen (56). Nonetheless, from a practical point of view, the cognitive deficits in TgCRND8 mice have three important attributes as follows: they occur early in life; they are easily detected in the conventional spatial reference memory version of the water maze; and they are sufficiently robust to be detected without recourse to large sample sizes.

Although overaccumulation of the Aβ peptide is firmly implicated in AD pathogenesis, the mechanisms leading to cognitive decline are not clear. As attempts to correlate plaque burdens and cognitive deterioration have produced mixed results (see Refs. 57–65 and also see Ref. 56), it is possible Aβ affects the central nervous system by mechanisms other than (or in addition to) the toxicity of extracellular, aggregated forms. Indeed, recent studies emphasize soluble forms of Aβ as crucial determinants of clinical outcome (50, 66, 67). Unfortunately, the molecular determinants for neurotoxicity (for example, free radical generating capacity of metal-bound Aβ42 (68, 69) and perturbed signal transduction (70)) and the cellular consequences thereof (altered synaptic function, excitotoxicity, and induction of apoptosis (49, 66)) are undetermined. We suggest TgCRND8 mice comprise a useful and validated system to address these issues. Amelioration of cognitive deficits by immunization against Aβ42 peptide (1) provides compelling evidence for a strong pathogenic role for Aβ peptide in the TgCRND8 model of AD and indeed for the amyloid cascade hypothesis. Parenthetically, these data effectively exclude the proposition that cognitive deficits in TgCRND8 mice derive from an insertional mutation. Furthermore, synthesis of antisera in Aβ42-immunized mice that react strongly with the peptide presented in a β-sheet conformation (1) suggests a potential to dissect the mechanism of Aβ neuropathogenesis (for example, by passive immunization (71) with conformation-specific antibodies). In short, the availability of a new AD model with robust cognitive deficits, levels of Aβ peptide that equal those seen in AD cases, and AD-like pathology may allow both an improved understanding of causal relationships between these phenotypic traits and testing of candidate interventions.

Acknowledgments—We thank Richard Rubenstein for generously supplying the 4G8 antibody, Frédéric Checler for the 3542 antibody, Sam Gandy for the 369 antibody, Julie Panakos for DNA microinjections, and Isabelle Aubert for discussions.

REFERENCES

1. Janus, C., Pearson, J., McLaurin, J., Mathews, P. M., Jiang, Y., Schmidt, S. D., Chishti, M. A., Horne, P., Heslin, D., French, J., Mount, H. T. J., Nixon, R. A., Mercken, M., Bergereon, C., Fraser, P. E., St. George-Hyslop, P., and

Downloaded from www.jbc.org at NATHAN S KLINE INSTITUTE, on December 6, 2012

Westaway, D. (2000) *Nature* **408,** 979–982
2. Citron, M., Oltersdorf, T., Haass, C., McConlogue, C., Hung, A. Y., Seubert, P., Vigo-Pelfrey, C., Lieberburg, I., and Selkoe, D. J. (1992) *Nature* **360,** 672–674
3. Roher, A. E., Lowenson, J. D., Clarke, S., Wolkow, C., Wang, R., Cotter, R. J., Reardon, I. L., Zurcher-Neely, H. A., Heinrikson, R. L., Ball, M. J., and Greenberg, B. D. (1993) *J. Biol. Chem.* **268,** 3072–3083
4. Johnston, J. A., Cowburn, R. F., Norgren, S., Wiehager, B., Venizelos, N., Winblad, B., Vigo-Pelfrey, C., Schenk, D., Lannfelt, L., and O'Neill, C. (1994) *FEBS Lett.* **354,** 274–278
5. Suzuki, N., Cheung, T. T., Cai, X.-D., Odaka, A., Otvos, L., Eckman, C., Golde, T., and Younkin, S. G. (1994) *Science* **264,** 1336–1340
6. Thinakaran, G., Teplow, D. B., Siman, R., Greenberg, B., and Sisodia, S. S. (1996) *J. Biol. Chem.* **271,** 9390–9397
7. Duff, K., Eckman, C., Zehr, C., Yu, X., Prada, C.-M., Perez-tur, J., Hutton, M., Buee, L., Harigaya, Y., Yager, D., Morgan, D., Gordon, M., Holcomb, L., Refolo, L., Zenk, B., Hardy, J., and Younkin, S. (1996) *Nature* **383,** 710–713
8. Borchelt, D. R., Thinakaran, G., Eckman, C. B., Lee, M. K., Davenport, F., Ratovitsky, T., Prada, C.-M., Kim, G., Seekins, S., Yager, D., Slunt, H. H., Wang, R., Seeger, M., Levey, A. I., Gandy, S. E., Copeland, N. G., Jenkins, N. A., Price, D. L., Younkin, S. G., and Sisodia, S. S. (1996) *Neuron* **17,** 1005–1013
9. Citron, M., Westaway, D., Xia, W., Carlson, G. A., Diehl, T., Levesque, G., Johnson-Wood, K., Lee, M., Seubert, P., Davis, A., Kholodenko, D., Motter, R., Sherrington, R., Perry, B., Yao, H., Strome, R., Lieberburg, I., Rommens, J., Kim, S., Schenk, D., Fraser, P., St. George-Hyslop, and Selkoe, D. (1997) *Nat. Med.* **3,** 67–72
10. Corder, E. H., Saunders, A. M., Srittmatter, W. J., Schmechel, D. E., Gaskell, P. C., Small, G. W., Roses, A. D., Haines, J. L., and Pericak-Vance, M. A. (1993) *Science* **261,** 921–923
11. Holtzman, D. M., Bales, K. R., Tenkova, T., Fagan, A. M., Parsadanian, M., Sartorius, L. J., Mackey, B., Olney, J., McKeel, D., Wozniak, D., and Paul, S. M. (2000) *Proc. Natl. Acad. Sci. U. S. A.* **97,** 2892–2897
12. Yankner, B. A., Duffy, L. K., and Kirschner, D. A. (1990) *Science* **250,** 279–282
13. Lorenzo, A., and Yankner, B. A. (1994) *Proc. Natl. Acad. Sci. U. S. A.* **91,** 12243–12247
14. Geula, C., Wu, C. K., Saroff, D., Lorenzo, A., Yuan, M., and Yankner, B. A. (1998) *Nat. Med.* **4,** 827–831
15. Hsiao, K. (1998) *Exp. Gerontol.* **33,** 883–889
16. Janus, C., Chishti, M. A., and Westaway, D. (2000) *Biochim. Biophys. Acta* **1502,** 63–75
17. Games, D., *et al.* (1995) *Nature* **373,** 523–527
18. Hsiao, K. H., Chapman, P., Nilsen, S., Eckman, C., Harigawa, Y., Younkin, S., Yang, F. S., and Cole, G. (1996) *Science* **274,** 99–102
19. Sturchler-Pierrat, C., Abramowski, D., Duke, M., Wiederhold, K. H., Mistl, C., Rothacher, S., Ledermann, B., Burki, K., Frey, P., Paganetti, P. A., Waridel, C., Calhoun, M. E., Jucker, M., Probst, A., Staufenbiel, M., and Sommer, B. (1997) *Proc. Natl. Acad. Sci. U. S. A.* **94,** 13287–13292
20. Calhoun, M. E., Wederhold, K.-H., Abramowski, D., Phinney, A. L., Probst, A., Sturchler-Pierrat, C., Staufenbiel, M., Sommer, B., and Jucker, M. (1998) *Nature* **395,** 755–756
21. Dodart, J. C., Mathis, C., Saura, J., Bales, K. R., Paul, S. M., and Ungerer, A. (2000) *Neurobiol. Dis.* **7,** 71–85
22. Hsiao, K. K., Borchelt, D. R., Olson, K., Johannsdottir, R., Kitt, C., Yunis, W., Xu, S., Eckman, C., Younkin, S., Price, D., Iadecola, C., Clark, H. B., and Carlson, G. A. (1995) *Neuron* **15,** 1203–1218
23. Moechars, D., Dewachter, I., Lorent, K., Reverse, D., Baekelandt, V., Naidu, A., Tesseur, I., Spittaels, K., Haute, C. V., Checler, F., Godaux, E., Cordell, B., and Van Leuven, F. (1999) *J. Biol. Chem.* **274,** 6483–6492
24. Chapman, P. F., White, G. L., Jones, M. W., Cooper-Blacketer, D., Marshall, V. J., Irizarry, M., Younkin, L., Good, M. A., Bliss, T. V., Hyman, B. T., Younkin, S. G., and Hsiao, K. K. (1999) *Nat. Neurosci.* **2,** 271–276
25. Dodart, J. C., Meziane, H., Mathis, C., Bales, K. R., Paul, S. M., and Ungerer, A. (1999) *Behav. Neurosci.* **113,** 982–990
26. Kang, J., Lemaire, H.-G., Unterbeck, A., Salbaum, J. M., Masters, C. L., Grzeschik, K.-H., Multhaup, G., Beyreuther, K., and Muller-Hill, B. (1987) *Nature* **325,** 733–736
27. Vieira, J., and Messing, J. (1982) *Gene* (*Amst.*) **19,** 259–268
28. Bolivar, F., Rodriguez, R. L., Greene, P. J., Betlach, M. C., Heyneker, H. L., and Boyer, H. W. (1977) *Gene* (*Amst.*) **2,** 95–113
29. Scott, M. R., Köhler, R., Foster, D., and Prusiner, S. B. (1992) *Protein Sci.* **1,** 986–997
30. Scott, M., Foster, D., Mirenda, C., Serban, D., Coufal, F., Wälchli, M., Torchia, M., Groth, D., Carlson, G., DeArmond, S. J., Westaway, D., and Prusiner, S. B. (1989) *Cell* **59,** 847–857
31. Johnson-Wood, K., Lee, M., Motter, R., Hu, K., Gordon, G., Barbour, R., Khan, K., Gordon, M., Tan, H., Games, D., Lieberburg, I., Schenk, D., Seubert, P., and McConlogue, L. (1997) *Proc. Natl. Acad. Sci. U. S. A.* **94,** 1550–1555
32. Haccou, P., and Meelis, E. (1995) *Statistical Analysis of Behavioural Data*, pp. 120–186 Oxford University Press, Oxford
33. Janus, C., D'Amelio, S., Amitay, O., Chishti, M. A., Strome, R., Fraser, P. E., Carlson, G. A., Roder, J., St. George-Hyslop, P., and Westaway, D. (2000) *Neurobiol. Dis.* **21,** 541–549
34. Gass, P., Wolfer, D. P., Balschun, D., Rudolph, D., Frey, U., Lipp, H. P., and Schutz, G. (1998) *Learn. Mem.* **5,** 274–88
35. Wehner, J. M., Sleight, S., and Upchurch, M. (1990) *Brain Res.* **523,** 181–187
36. Carlson, G. A., Borchelt, D. R., Dake, A., Turner, S., Danielson, V., Coffin, J. D., Eckman, C., Meiners, J., Nilsen, S. P., Younkin, S. G., and Hsiao, K. K. (1997) *Hum. Mol. Genet.* **6,** 1951–1959
37. Iadecola, C., Zhang, F., Niwa, K., Eckman, C., Turner, S. K., Fischer, E., Younkin, S., Borchelt, D. R., Hsiao, K. K., and Carlson, G. A. (1999) *Nat. Neurosci.* **2,** 157–161
38. Telling, G. C., Scott, M., Mastrianni, J., Gabizon, R., Torchia, M., Cohen, F. E., DeArmond, S. J., and Prusiner, S. B. (1995) *Cell* **83,** 79–90
39. Moser, M., Colello, R. J., Pott, U., and Oesch, B. (1995) *Neuron* **14,** 509–517
40. DeArmond, S. J., Sanchez, H., Yehiely, F., Qiu, Y., Ninchak-Casey, A., Daggett, V., Camerino, A. P., Cayetano, J., Rogers, M., Groth, D., Torchia, M., Tremblay, P., Scott, M. R., Cohen, F. E., and Prusiner, S. B. (1997) *Neuron* **19,** 1337–1348
41. Irizarry, M. C., McNamara, M., Fedorchak, K., Hsiao, K., and Hyman, B. T. (1997) *J. Neuropathol. Exp. Neurol.* **56,** 965–973
42. Kim, K. W., Miller, D. L., Sapienza, V. J., Chen, C. M. J., Bai, C., Grundke-Iqbal, I., Currie, J. R., and Wisnieski, H. M. (1988) *Neurosci. Res. Commun* **2,** 121–130
43. Spillantini, M. G., Goedert, M., Jakes, R., and Klug, A. (1990) *Proc. Natl. Acad. Sci. U. S. A.* **87,** 3947–3951
44. Oesch, B., Westaway, D., Wälchli, M., McKinley, M. P., Kent, S. B. H., Aebersold, R., Barry, R. A., Tempst, P., Teplow, D. B., Hood, L. E., Prusiner, S. B., and Weissmann, C. (1985) *Cell* **40,** 735–746
45. Braak, H., and Braak, E. (1991) *Acta Neuropathol.* **82,** 239–259
46. Citron, M., Eckman, C. B., Diehl, T. S., Corcoran, C., Ostaszewski, B. L., Xia, W., Levesque, G., St. George-Hyslop, P., Younkin, S. G., and Selkoe, D. J. (1998) *Neurobiol. Dis.* **5,** 107–116
47. Storey, E., and Cappai, R. (1999) *Neuropathol. Appl. Neurobiol.* **25,** 81–97
48. Sherrington, R., Rogaev, E., Liang, Y., Rogaeva, E., Levesque, G., Ikeda, M., Chi, H., Lin, C., Holman, K., Tsuda, T., Mar, L., Fraser, P., Rommens, J. M., and St. George-Hyslop, P. (1995) *Nature* **375,** 754–760
49. Hsia, A. Y., Masliah, E., McConlogue, L., Yu, G. Q., Tatsuno, G., Hu, K., Kholodenko, D., Malenka, R. C., Nicoll, R. A., and Mucke, L. (1999) *Proc. Natl. Acad. Sci. U. S. A.* **96,** 3228–3233
50. Wang, J., Dickson, D. W., Trojanowski, J. Q., and Lee, V. M. (1999) *Exp. Neurol.* **158,** 328–337
51. Mucke, L., Masliah, E., Yu, G. Q., Mallory, M., Rockenstein, E. M., Tatsuno, G., Hu, K., Kholodenko, D., Johnson-Wood, K., and McConlogue, L. (2000) *J. Neurosci.* **20,** 4050–4058
52. Masliah, E., Sisk, A., Mallory, M., Mucke, L., Schenk, D., and Games, D. (1996) *J. Neurosci.* **16,** 5795–5811
53. Irizarry, M. C., McNamara, M., Page, K. J., Schenk, D., Games, D., and Hyman, B. T. (1997) *J. Neurosci.* **17,** 7053–7059
54. Patrick, G. N., Zukerberg, L., Nikolic, M., de la Monte, S., Dikkes, P., and Tsai, L. H. (1999) *Nature* **402,** 615–622
55. Ahlijanian, M. K., Barrezueta, N. X., Williams, R. D., Jakowski, A., Kowsz, K. P., McCarthy, S., Coskran, T., Carlo, A., Seymour, P. A., Burkhardt, J. E., Nelson, R. B., and McNeish, J. D. (2000) *Proc. Natl. Acad. Sci. U. S. A.* **97,** 2910–2915
56. Chen, G., Chen, K. S., Knox, J., Inglis, J., Bernard, A., Martin, S. J., Justice, A., McConlogue, L., Games, D., Freedman, S. B., and Morris, R. G. (2000) *Nature* **408,** 975–979
57. Masliah, E., Terry, R. D., Alford, M., DeTeresa, R. M., and Hansen, L. A. (1991) *Am. J. Pathol.* **138,** 235–246
58. Terry, R. D., Masliah, E., Salmon, D. P., Butters, N., DeTeresa, R., Hill, R., Hansen, L. A., and Katzman, R. (1991) *Ann. Neurol.* **30,** 572–580
59. Arriagada, P. V., Growdon, J. H., Hedley-Whyte, E. T., and Hyman, B. T. (1992) *Neurology* **42,** 631–639
60. Terry, R. D. (1996) *J. Neuropathol. Exp. Neurol.* **55,** 1023–1025
61. Cummings, B. J., Pike, C. J., Shankle, R., and Cotman, C. W. (1996) *Neurobiol. Aging* **17,** 921–933
62. Gomez-Isla, T., Hollister, R., West, H., Mui, S., Growdon, J. H., Petersen, R. C., Parisi, J. E., and Hyman, B. T. (1997) *Ann. Neurol.* **41,** 17–24
63. Bartoo, G. T., Nochlin, D., Chang, D., Kim, Y., and Sumi, S. M. (1997) *J. Neuropathol. Exp. Neurol.* **56,** 531–540
64. Crook, R., Verkkoneimi, A., Perez-Tur, J., Mehta, N., Baker, M., Houlden, H., Farrer, M., Hutton, M., Lincoln, S., Hardy, J., Gwinn, K., Somer, M., Paetau, A., Kalimo, H., Ylikoski, R., Poyhonen, M., Kucera, S., and Haltia, M. (1998) *Nat. Med.* **4,** 452–455
65. Beach, T. G., Kuo, Y. M., Spiegel, K., Emmerling, M. R., Sue, L. I., Kokjohn, K., and Roher, A. E. (2000) *J. Neuropathol. Exp. Neurol.* **59,** 308–313
66. Lue, L. F., Kuo, Y. M., Roher, A. E., Brachova, L., Shen, Y., Sue, L., Beach, T., Kurth, J. H., Rydel, R. E., and Rogers, J. (1999) *Am. J. Pathol.* **155,** 853–862
67. McLean, C. A., Cherny, R. A., Fraser, F. W., Fuller, S. J., Smith, M. J., Beyreuther, K., Bush, A. I., and Masters, C. L. (1999) *Ann. Neurol.* **46,** 860–866
68. Huang, X., Atwood, C. S., Hartshorn, M. A., Multhaup, G., Goldstein, L. E., Scarpa, R. C., Cuajungco, M. P., Gray, D. N., Lim, J., Moir, R. D., Tanzi, R. E., and Bush, A. I. (1999) *Biochemistry* **38,** 7609–7616
69. Huang, X., Cuajungco, M. P., Atwood, C. S., Hartshorn, M. A., Tyndall, J. D., Hanson, G. R., Stokes, K. C., Leopold, M., Multhaup, G., Goldstein, L. E., Scarpa, R. C., Saunders, A. J., Lim, J., Moir, R. D., Glabe, C., Bowden, E. F., Masters, C. L., Fairlie, D. P., Tanzi, R. E., and Bush, A. I. (1999) *J. Biol. Chem.* **274,** 37111–37116
70. Harkany, T., Abraham, I., Konya, C., Nyakas, C., Zarandi, M., Penke, B., and Luiten, P. G. (2000) *Rev. Neurosci.* **11,** 329–382
71. Bard, F., Cannon, C., Barbour, R., Burke, R.-L., Games, D., Grajeda, H., Guido, T., Hu, K., Huang, J., Johnson-Wood, K., Khan, K., Kholodenko, D., Lee, M., Lieberburg, I., Motter, R., Nguyen, M., Soriano, F., Vasquez, N., Weiss, K., Welch, B., Seubert, P., Schenk, D., and Yednock, T. (2000) *Nat. Med.* **6,** 916–919
72. Capell, A., Saffrich, R., Olivo, J.-C., Meyn, L., Walter, J., Grunberg, J., Dotti, C., and Haass, C. (1997) *J. Neurochem.* **69,** 2432–2340
73. Dewachter, I., Van Dorpe, J., Smeijers, L., Gilis, M., Kuiperi, C., Laenen, I., Caluwaerts, N., Moechars, D., Checler, F., Vanderstichele, H., and Van Leuven, F. (2000) *J. Neurosci.* **20,** 6452–6458

Downloaded from www.jbc.org at NATHAN S KLINE INSTITUTE, on December 6, 2012